Spectral mapping methods applied to LiDAR data: Application to fuel type mapping

Margarita Huesca[a,*], David Riaño[b,c], Susan L. Ustin[b]

[a] *Center for Spatial Technologies And Remote Sensing (CSTARS), John Muir Institute of the Environment, University of California Davis, USA*
[b] *Center for Spatial Technologies And Remote Sensing (CSTARS), Department of Land, Air, and Water Resources, University of California Davis, USA*
[c] *Instituto de Economía, Geografía y Demografía (IEGD), Centro de Ciencias Humanas y Sociales (CCHS), Consejo Superior de Investigaciones Científicas (CSIC), Albasanz 26-28 28037 Madrid, Spain*

A B S T R A C T

Originally developed to classify multispectral and hyperspectral images, spectral mapping methods were used to classify Light Detection and Ranging (LiDAR) data to estimate the vertical structure of vegetation for Fuel Type (FT) mapping. Three spectral mapping methods generated spatially comprehensive FT maps for Cabañeros National Park (Spain): (1) Spectral Mixture Analysis (SMA), (2) Spectral Angle Mapper (SAM), and (3) Multiple Endmember Spectral Mixture Analysis (MESMA). The Vegetation Vertical Profiles (VVPs) describe the vertical distribution of the vegetation and are used to define each FT endmember in a LiDAR signature library. Two different approaches were used to define the endmembers, one based on the field data collected in 1998 and 1999 (Approach 1) and the other on exploring spatial patterns of the singular FT discriminating factors (Approach 2). The overall accuracy is higher for Approach 2 and with best results when considering a five-FT model rather than a seven-FT model. The agreement with field data of 44% for MESMA and SMA and 40% for SAM is higher than the 38% of the official Cabañeros National Park FTs map. The principal spatial patterns for the different FTs were well captured, demonstrating the value of this novel approach using spectral mapping methods applied to LiDAR data. The error sources included the time gap between field data and LiDAR acquisition, the steep topography in parts of the study site, and the low LiDAR point density among others.

1. Introduction

Vegetation structure can be directly measured using Light Detection and Ranging (LiDAR) data (Gajardo et al., 2014), which is an essential parameter for many environmental issues such as ecosystem function and forest fire monitoring, among others. This type of information is generally defined by metrics that provide information about components of vegetation structure like height, crown width, and crown base height. This paper explores a new application to extract information from LiDAR data, using spectral mapping methods originally developed to classify multispectral or hyperspectral images. Among the spectral mapping methods, Spectral Mixture Analysis (SMA) (Smith et al., 1990a,b), Spectral Angle Mapper (SAM) (Kruse et al., 1993), Multiple Endmember Spectral Mixture Analysis (MESMA) (Dennison and Roberts, 2003; Roberts et al., 1998) have successfully mapped vegetation. These methods require identification of pure spectral signatures (i.e., endmembers) to characterize each class, which can be extracted from a field survey, a library, or from the actual image. Taking advantage of the penetration capability of LiDAR data, this study builds Vegetation Vertical Profiles (VVP) to characterize different structural patterns that we treat as "endmembers".

To demonstrate the usefulness of spectral mapping, these methods were tested in the context of wildfires that have become major natural hazards across global landscapes. Among the factors that drive fire ignition and propagation (i.e., fuel condition, weather, and topography) (Pyne, 1996) managers can only control fuel accumulation (Pyne, 1996). Therefore, having an accurate and updated spatial distribution of fuels is essential to assess fire risk and behavior and to plan management activities (Burgan and Shasby, 1984). Depending on the fire propagation element, its height, and fuel density, Fuel Types (FTs) are grouped into vegetation classes based on their predicted fire behavior. Among the ones widely used in USA, Scott and Burgan (2005) extended the Northern Forest Fire Laboratory (NFFL; Albini, 1976) classification. In Europe, the Prometheus project (Prometheus, 1999) defined seven

---

FTs adapting the NFFL system to Mediterranean vegetation.

The complexity of fuels, in terms of their structure and dynamics, makes field surveys challenging and expensive. Remote sensing methods provide the necessary temporal, spectral and spatial coverage for FT mapping. Most of the studies done today are based on medium to high spatial resolution and low temporal resolution passive multi-spectral remote sensing images (Riaño et al., 2002; van Wagtendonk and Root, 2003) and few use hyperspectral data (Jia et al., 2006; Lasaponara et al., 2006). However, these passive remote sensing data products are based on vegetation optical properties that are not directly related to its vertical structure, which is the key attribute to discriminate FTs. For instance, Riaño et al. (2002) found problems using Landsat-TM data to discriminate among shrub FTs that differed only in shrub height. They also could not distinguish canopy FTs with and without an overstory. LiDAR data has been used before to classify FTs (García et al., 2011; Riaño et al., 2003; Hermosilla et al., 2014) and canopy fuel properties (e.g. Erdody and Moskal, 2010; Riaño et al., 2003, 2004; Zhao et al., 2011; Andersen et al., 2005), but the novelty of this study relies on the method used to analyze LiDAR data. This is the first study to apply spectral mapping methods to map FTs or other types of forest properties from LiDAR data. Spectral-based signatures record the reflectance of the object in many contiguous narrow spectral bands in the optical domain (400–2500 nm). However, instead of using spectral bands, these spectral mapping methods are applied to the LiDAR VVPs that are based on the energy at each height interval. The specific objectives are to create a LiDAR signature library that is used to define FTs and to build a spatially comprehensive FTs map for Cabañeros National Park based on the Prometheus classification.

2. Study site

Cabañeros National Park (Fig. 1) is situated in the western part of the southern plateau of Spain. Cabañeros covers approximately 41,000 ha. It has complex topography with 900–1400 m elevation above sea level in the mountainous areas and 500–700 m in the valley.

It is a warm temperate inland Mediterranean climate, ranging from 13 °C to 16 °C mean annual temperatures and 500–850 mm/year annual rainfall. Winter is cold and rainy, spring and fall are wet and short, and summer is hot and dry. However, climatic conditions vary locally due to topography.

Drought tolerant evergreen holm oak (*Quercus ilex* L.) and cork oak (*Q. suber* L.), and semi-evergreen oak gall oak (*Q. faginea* Lam.) dominate Cabañeros. The complex topography together with variable climatic conditions results in varying vegetation types distributed across the study site. Large grazed pastures characterize the low elevation, low relief fields, while tall grass species are dispersed with holm oak (i.e., in woodlands or "dehesas"). Steeper mountainous areas contain *Q. faginea* and *Q. pyrenaica* Willd. High elevations or deep valley soils with high water levels include *Q. pyrenaica* and the deciduous tree *Sorbus torminalis* (L.) Crantz. *Q. ilex* and *Q. suber* grow in drier areas and *Heliophilae* species dominate degraded areas such as perennial shrubs, rock roses (*Cistus ladanifer* L., *Cistus populifolius* L.) and low growing perennial shrub heather (*Erica australis* L., *Erica umbellata* Loefl. ex L. and *Erica arborea* L.).

3. Data and methods

3.1. Field data collection

Field campaigns during the years 1998 and 1999 collected data over a hundred plots distributed across Cabañeros. Each plot within a 200 × 200 m area, represents a homogeneous FT following the Prometheus system (Prometheus, 1999). The Prometheus system is mainly based on the type and the height of the fire propagation element, adapted to Southern European vegetation. The system defines seven FTs described in Table 1.

The number of selected plots (200 × 200 m) per FT was proportional to the surface area occupied by each FT (Table 2). The center of each plot was recorded using a GARMIN-12-Map GPS. This instrument had a Root Mean Square Error of 43 m, calculated after measuring the
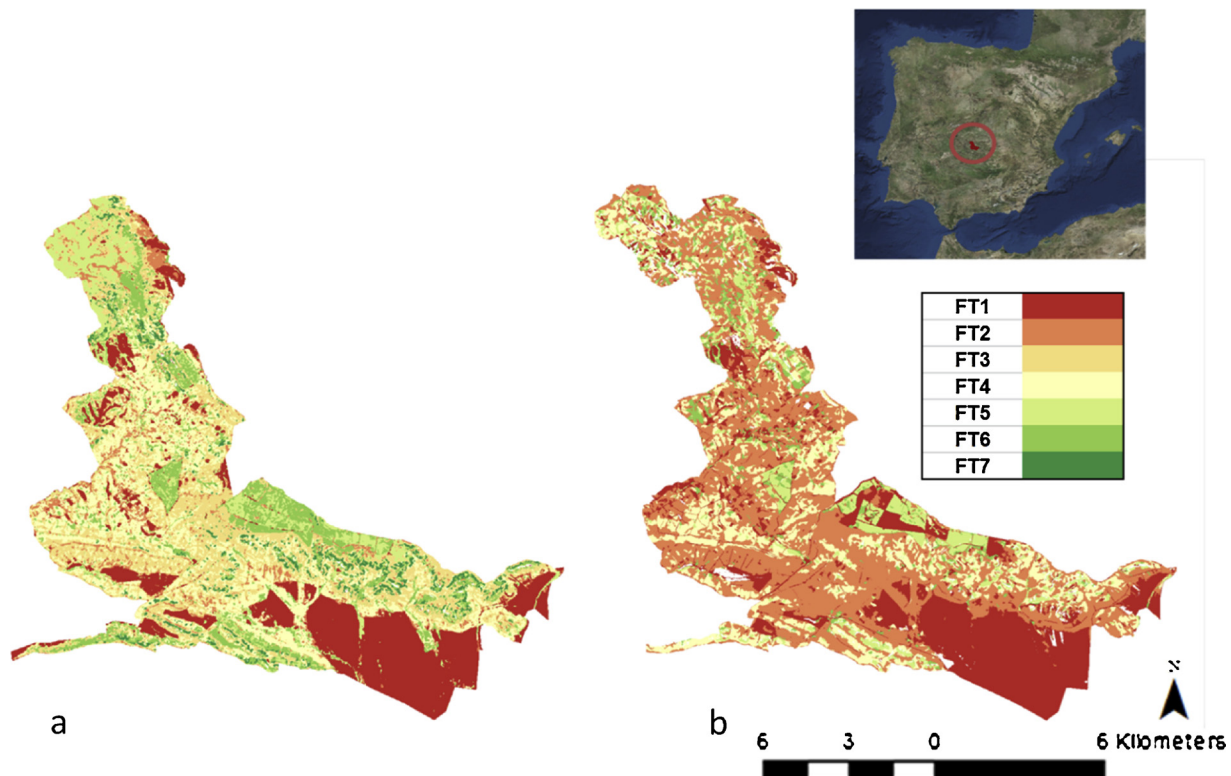

Fig. 1. Riaño et al (2002) (a) and CLM (b) FT maps. Coordinates in latitude/longitude: Upper left corner: 39.59 N, 4.74 W; Lower right corner; 39.27 N, 4.19 E.

Table 1

The seven fuel types defined by Prometheus system.

Fuel name	Fuel Type	Cover			Shrubs mean height	Difference between shrubs and trees
		grass	shrub	trees		
Ground fuels	F1	> 60%				
Surface fuels	F2		> 60%	< 50%	0.30-0.60 m	
Medium-height shrubs	F3		> 60%	< 50%	0.60-2.00 m	
Tall shrubs	F4		> 60%	< 50%	2.00-4.00 m	
Tree stands with clear surface fuels	F5		< 30%	> 50%		
Tree stands with medium surface fuels	F6		> 30%	> 50%		> 0.5 m
Tree stands with heavy surface fuels	F7		> 30%	> 50%		< 0.5 m

Table 2

Number of plots per FT during the fields campaigns 1998–1999 and 2000.

FT	1998-1999	2000
1	14	12
2	6	10
3	26	31
4	17	34
5	14	15
6	17	17
7	6	9
Total	**100**	**128**

same location on 17 different days and compared to an ASHTECH-*Z*-Surveyor dual frequency geodesic GPS. The ASHTECH-*Z*-Surveyor has an estimated error of less than 1 m, if measured for 20 min observation time. Each sampling plot recorded the dominant vegetation species, density, coverage, height, elevation, slope, solar incident angle, location, and acquisition date. Four plots were outside the National Park boundary, so they were removed from this analysis. During the year 2000, ASHTECH-Z-Surveyor registered 128 additional plots that were used for validation.

3.2. LiDAR preprocessing

Spanish National Plan of Aerial Orthophotography (PNOA) (http://www.ign.es/PNOA/vuelo_lidar.html) collected small footprint discrete return-recording LiDAR data in 2009 using a Leica ALS60 sensor. The data has a point density of ~0.5 pts/m^2 with a vertical accuracy better than 0.20 m. The raw data points are in 2×2 km tiles of unclassified points in LAS binary format and UTM Zone 30 ETRS 1989 projection. A bare earth Digital Elevation Model (DEM), provided by PNOA at 5 m spatial resolution, was used to normalize the height of LiDAR returns to heights above ground.

The command "groundfilter" from FUSION v.3.42 software (developed at the U.S. Forest Service Pacific Northwest Research Station), generated a bare-earth surface after filtering ground and non-ground points from the raw data. The function uses an algorithm based on Kraus and Pfeifer (1998). Vegetation returns are removed using a weighting function with appropriate coefficients estimated with sufficient interactions. Finally, the VVP was computed to describe the vertical distribution of the vegetation at a 0.5 m vertical resolution, as the proportion of canopy returns for each height bin within a 30 m pixel grid.

3.3. Spectral mapping methods to generate the FTs map

This study tested three spectral mapping methods, originally developed to classify vegetation for hyperspectral images, to generate FT maps from LiDAR data: Spectral Mixture Analysis (SMA; Smith et al., 1990a,b), Spectral Angle Mapper (SAM; Kruse et al., 1993), and Multiple Endmember Spectral Mixture Analysis (MESMA; Roberts et al., 1998; Dennison et al., 2004). Each classifier method is based on defined

pure spectral components or endmembers. Usually these endmembers are spectral signatures from vegetation reflectance in the optical domain (400–2500 nm). Instead, here the VVPs are used to define the LiDAR endmembers. The two unmixing procedures tested the hypothesis that at pixel scales most pixels are a mix of fuel types. We classified each pixel based on the dominant fuel type. The SAM classifier was selected based on the assumption that each fuel type is characterized by a different VVP shape, independent of the absolute values at each height interval. The SAM procedure calculates the angle between two spectral signatures to determine how similar are their shapes.

SMA and MESMA model each pixel as a linear combination of the fraction of each endmember and assigns the class with the highest fraction from the models having the lowest error. The main difference between them is that in MESMA the numbers and types of endmembers can vary at the pixel level (Roberts et al., 1998). By contrast, SAM is a vector comparison method. It considers each pixel as an n-dimensional vector. A small angle between the endmember and the pixel signal indicates high similarity and assigns the endmember to the class with the smallest angle. MESMA constrains the maximum allowable RMSE to 2.5%. The minimum and maximum allowable endmember fractions fall between −0.05 and 1.05. SMA and SAM are implemented in EVI/IDL software and MESMA in ENVI/IDL VIPER Tools, an add on package (Roberts et al., 2007).

3.4. Endmember selection

Two approaches defined the VVP signature that represents each FT i.e., endmember. The first is based on the fieldwork collected in 1998 and 1999. Each field plot is defined by one VVP signature using regions of interests (i.e. mean value of the 30-m pixels within the 200×200 m plot). Three metrics were selected to represent the VVP endmember, using the VVP signatures from the field plots: (1) Count-based Endmember Selection (COB: Roberts et al., 2003), the maximum number of VVP signatures that can be modeled within a class (inCOB) determines the endmember; (2) Endmember average RMSE (EAR: Dennison and Roberts, 2003), in which the minimum RMSE within a class determines the endmember; and (3) Minimum Average Spectral Angle (MASA: Dennison et al., 2004), the lowest average spectral angle determines this endmember. The final endmember for a FT was one with high inCOB and low MASA and EAR values. The second approach we used identified each FT through visual exploration of the VVP profiles obtained from the image. The most distinct profiles were selected; they were grouped based on the characteristic of each FT in terms of fuel height, and distance between the ground surface and canopy fuels. Several VVP profiles per FT were selected in a final step, among the possible VVP patterns; SAM was used to evaluate their dissimilarity and ranked the match for each endmember against the others. A score of 1 indicates a perfect match and a score of 0 means they are totally different. At the end one VVP profile was chosen to characterize each FT.

Table 3
Prometheus and Rothermel FT classifications equivalence.

Prometheus	Rothermel
FT1	Models 1 (short grass), 2 (medium grass) and 3 (tall grass)
FT2	Model 5 (shrub height lower than 0.6 m)
FT3	Model 6 (shrub height between 0.6-1.2 m)
FT4	Model 4(dense shrub with mean height higher than 2 m)
FT5	Models 8 and 9 (closed timber liter)
FT6	Model 10 (litter with presence of herbaceous and shrub understory)
FT7	Model 7 (dense shrub under tree canopy)

3.5. Validation

In the first phase, a 7-FT map was generated using the two endmember approaches and the three spectral mapping methods. The field work collected in 1998–1999 and in 2000 found that FTs 2 and 7 were under represented within the study area and consequently they were dropped. Therefore, a second phase applied the three classification methods to the five dominant FTs. Congalton and Green's (1999) accuracy assessment was used to validate the FT maps using the field plots collected in 2000 in confusion matrixes. In addition, results were compared to two available FT maps of the park (Fig. 1) to evaluate the spatial coherence of the FTs. Riaño et al. (2002) generated a Prometheus FT classification map using Landsat-TM, ancillary topographic variables and only 1998–1999 field plots, shown in Table 2. The Castilla-La Mancha region (CLM) (Spain) delivered an official FT product in 2016 obtained from Digital Orthophotos and field plots sampled in 2016 from the 2009 PNOA LiDAR data used in this study. Prometheus was not directly used because CLM applied the Rothermel (1972) classification thus; the equivalence between these two FT classifications is shown in Table 3, which made it possible to make a direct comparison.

The Riaño et al. (2002) FT map discriminated the seven Prometheus FTs. The CLM map shows that FT3 and FT7 were not present. The FT2 and FT3 are similar classes (i.e. shrub FTs with average heights below or above 0.6 m), therefore, this study assumes that FT2 in CLM's map corresponds with FT3 in Riaño's map for validation purposes. Confusion matrixes evaluated the accuracy of these maps compared to the 2000 field data shown in Table 2. The perimeter of Riaño's map is smaller than CLM's map because it was created when the northwest area was not yet included within the National Park. Therefore, Riaño's perimeter was used to compare their map to our results whereas CLM's perimeter compared between CLM's map and our results.

4. Results

Approach 1 selected the endmember that represented each FT using the statistics inCOB, MASA and EAR applied to the different VVPs within a FT (Fig. 2). It is important to note that the largest number of VVP (%) represents the smallest plant sizes and the numbers decline as plants size get bigger.

FT1 concentrates most of the returns from very low heights. FTs associated with shrubs (i.e. FT2, FT3 and FT4) present similar VVP profiles with high percentages of returns from very low heights and some at medium height and a few at high height intervals. The differences among them are that FT2 has the highest percentages of returns at the lowest heights and the lowest percentage at medium heights, whereas the opposite occurs in FT4. FT3 has intermediate patterns between FT2 and FT4. The main characteristic of FTs associated with tree stands (i.e. FT5, FT6 and FT7) is the presence of returns at tall height intervals. The percentage of tall heights is least in relation to other height intervals, but never zero, as occurs in FTs associated with grasses and shrubs. The differences among these tree stand FTs is that the percentage of returns is small at low heights, and increases at

medium height intervals from FT5 to FT7.

The differences among endmembers are more noticeable following Approach 2 (Fig. 3) than Approach 1. Nevertheless, the general FTs characteristics associated with grass, shrubs or tree stands are similar in both approaches. The grass FTs presents all returns at very low heights, shrub FTs show high percentage of returns at low and medium heights, and neither (i.e. grass and shrub FTs) show any returns at tall height intervals. Meanwhile, FTs associated with tree stands present returns along all height intervals and the percentage at very low height intervals is much less than in the other FTs. The difference among shrub FTs is clearer in Approach 2 than in Approach 1. The percentage of returns at medium height intervals increases from FT2 to FT4. The differences among tree stand FTs are even more remarkable than in Approach 1. Low returns at low heights, almost no returns in medium heights and high percentage of returns at tall height intervals characterize FT5. Similarly to FT5, FT6 shows low returns at low heights, but it presents more returns at medium heights and lower percentage of returns at tall height intervals. FT7 has many more returns at medium heights than the other two tree stand FTs but a lower percentage at tall height intervals. The similarity ranking showed that the endmembers selected are sufficiently distinct, especially when using the approach 2 (Table 4). Approach 1 shows higher similarity between FT5 and FT3, followed by FT7 and FT5.

Considering Approach 1 for endmember selection, seven-FTs tends to overestimate FT7, especially using SMA (Fig. 4). The highest accuracy is found with FT1 associated with grass. However, including just the five dominant FTs the accuracy improves for all three mapping methods. The SMA five-FT map tends to overestimate FTs related to tree stands (i.e. FT5 and FT6), while SAM and MESMA tend to underestimate them. FT1 had the highest accuracies for all three methods, but with a clear overestimation in MESMA.

Considering Approach 2 (Fig. 5), seven-FT maps tended to overestimate FT7, especially using SMA and SAM, but this overestimation is less than that for Approach 1. FT1 also produces the best accuracy. The Five-FT maps improved accuracy noticeably in all three mapping methods, especially with SMA. SMA and SAM capture the spatial distribution of all FTs, while MESMA tends to overestimate FT1.

In seven-FT classifications (Tables 6 and 7), FT7 is clearly overestimated, especially in SMA Approach 1. The least overestimation with MESMA is Approach 2. FT1 had the best accuracy in both approaches. FTs 5 and 6 are underestimated. FTs related to shrubs presented more errors among each other. Approach 2 shows least overestimation of FT1 and underestimation of FTs 5 and 6. Five-FT classifications in Tables 8 and 9 show that FTs related to trees are overestimated with the SMA Approach 1. SAM and MESMA tend to overestimate FTs related to shrubs. FT1 had the highest accuracy although it is clearly overestimated using MESMA, in Approach 2. The best results are found using SMA method and Approach 2 for endmember selection. Most errors occur within the shrub classes and within tree classes, while errors between grass, shrubs and tree classes are negligible.

5. Discussion

This research adapts LiDAR data to widely applied techniques used to classify vegetation from multispectral and more commonly with hyperspectral airborne imagery. Specifically, it tested three different spectral mapping methods, SMA, SAM and MESMA. The agreements obtained using three different datasets for validation (i.e. Riaño's map, CLM's map, and field data) demonstrate the potential efficacy for each of these techniques with LiDAR data. One of the main problems in using currently available FT maps for validation is that they are based on optical data metrics from satellite data (such as NDVI) that are only indirectly related to the vertical fuel structure. For instance, the Landscape Fire and Resource Planning Tools program (LANDFIRE) provides fuel data at US national level primarily based on assumptions between vegetation indices and height using Landsat and ecological
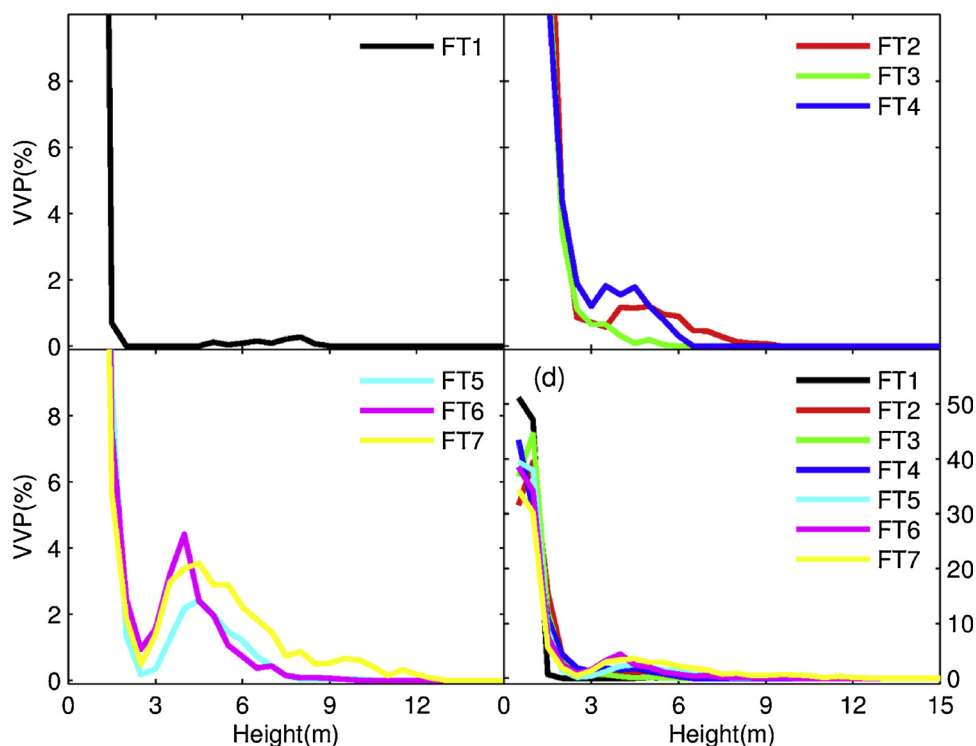
Fig. 2. Endmember selection (i.e. selected Vegetation Vertical Profiles (VVP)) using Approach 1 for FT1 (a), FT2, FT3 and FT4 (b), FT5, FT6 and FT7 (c), and all FTs (d).
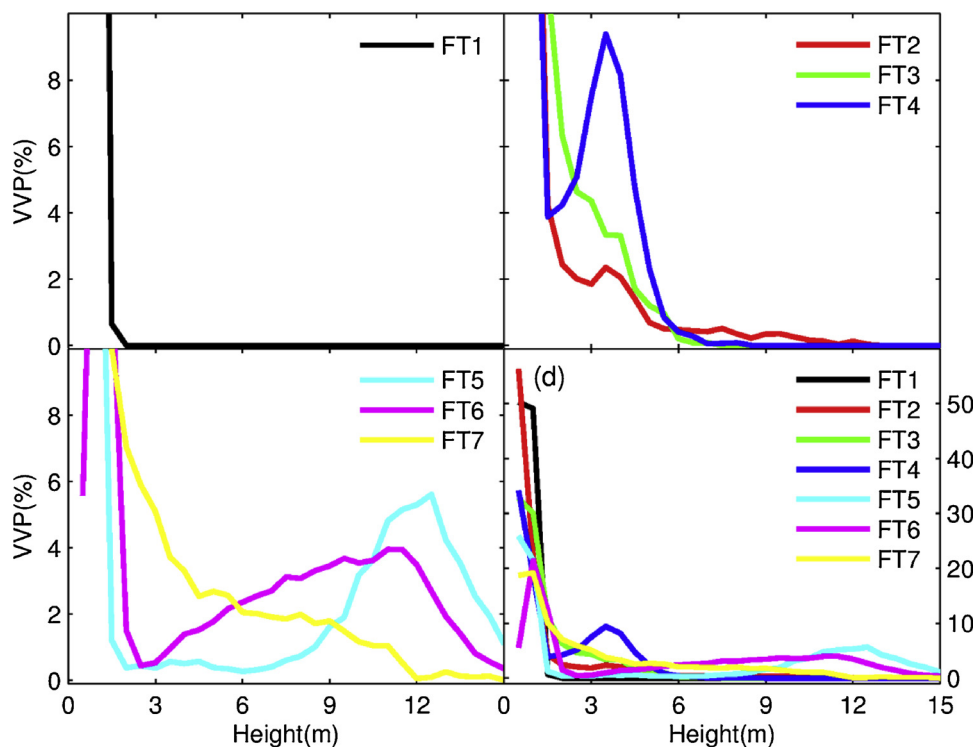
Fig. 3. Endmember selection (i.e. selected Vegetation Vertical Profiles (VVP)) using Approach 2 for FT1 (a), FT2, FT3 and FT4 (b), FT5, FT6 and FT7 (c), and all FTs (d).

models. The LANDFIRE program does not incorporate LiDAR, because it is not available at the national scale, although Peterson et al. (2015) has developed a tool (CHISLIC) to automatically integrate LiDAR into LANDFIRE that provides accurate local maps of FT.

The novelty of this research is two-fold, first it creates a general LiDAR signature library for defining FTs and second it uses LiDAR VVP for classifications via spectral mapping methods. Although more accurate FT maps could be developed using a combination of optical and LiDAR data (e.g., Garcia et al. 2011; Peterson et al., 2015), the principle goal of this research was to develop and test whether spectral methods

Table 4

Similarity ranking for endmembers evaluated with SAM using Approach 1 and Approach 2. A score of 1 indicates a perfect match and a score of 0 means they are unrelated.

	FT1	FT2	FT3	FT4	FT5	FT6	FT7
Approach 1							
FT1	1.00	0.00	0.49	0.35	0.55	0.00	0.54
FT2		1.00	0.00	0.00	0.00	0.50	0.00
FT3			1.00	0.49	0.72	0.00	0.48
FT4				1.00	0.47	0.00	0.48
FT5					1.00	0.00	0.69
FT6						1.00	0.00
FT7							1.00
Approach 2							
FT1	1.00	0.00	0.00	0.00	0.00	0.00	0.00
FT2		1.00	0.00	0.11	0.00	0.00	0.45
FT3			1.00	0.00	0.00	0.00	0.00
FT4				1.00	0.00	0.00	0.00
FT5					1.00	0.00	0.00
FT6						1.00	0.00
FT7							1.00

could be adapted for analyzing LiDAR data and to demonstrate its potential to produce improved FT maps.

While previous studies have shown that LiDAR data can discriminate vertical fuel structures (García et al., 2011; Riaño et al., 2003; Hermosilla et al., 2014), these approaches require training on local conditions, creating a challenge to replicate them at multiple sites over a broader scale. In contrast, the approach demonstrated here using LiDAR signatures could be easily applied to other areas to allow FT maps to be produced across a broader scale. This method benefits the upcoming spaceborne LiDAR opportunities, including the GEDI instrument expected on the International Space Station by November 2018, to generate and systematically update FT maps. The availability of this data for timely FT maps will provide information for better decision-making and risk mitigation. The LiDAR FT signature library was generated using field data that identified unique FT patterns related to structural differences. Results show that using VVP to define

endmembers is a promising option for classifying FTs accurately and comprehensively. Densities at each height interval determine the number of non-ground points relative to the total number of returns at each pixel. However, differences using the two approaches to discriminate endmembers show the importance of careful selection of endmembers to produce good performance using these methods.

Accuracies found in the validation process were better for Approach 2 than for Approach 1. MESMA performed better with Approach 1, while SMA and SAM had higher accuracies using Approach 2. The main spatial patterns for the different FTs within the study site were well captured for all of the five-FT classifications. This makes our approach potentially operational for forest managers. The seven-FT class maps were less accurate and clearly over or underestimated some FTs. However, the two additional FT classes included in the seven-FT maps were poorly represented in this study site, which may have influenced these results. Also it is important to note that the degree of agreement with field data was 44% for MESMA and SMA and 40% for SAM, as reported in Table 5, is higher than the 38% agreement between field data and the official CLM FT map, although the differences are not statistically significant.

To further evaluate the accuracy of the results presented here, it is important to consider the error sources. There is a time gap of approximately nine years between field data collection and LiDAR acquisition. Although Cabañeros is dominated by mature forest, abandonment of lands in the area has increased the percentage of shrubs. In addition, vegetation changes are expected due to small forest fires that have occurred in the area. This time lag could be especially relevant among shrubs FTs, as they are likely larger now than during field measurements and also among the tree stand FTs due to changes in understory conditions. Another issue is the complex topography in the north part of the study site that can affect LiDAR signals (Valbuena et al., 2011). For instance, ground returns in steep areas may be mistaken with vegetation returns, or very dense vegetation could be identified as ground (Riaño et al., 2007). The better spatial accuracy of today's GPS systems would likely improve the accuracies reported here.

The comparison between Riaño's and CLM's maps were analyzed pixel by pixel, which contributes to coregistration errors. Correlation
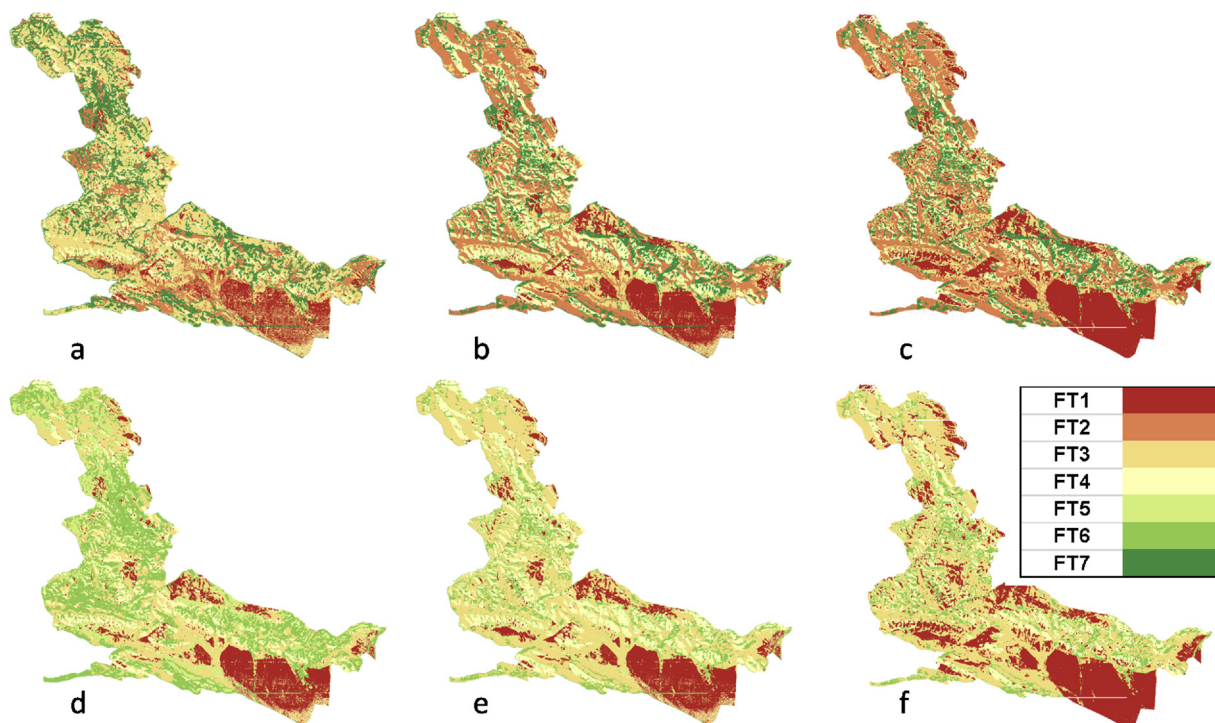

Fig. 4. Seven-FT (a, b, c) and five-FT (d, e, f) classifications using Approach 1 with SMA (a, d), SAM (b, e) and MESMA (c, f).
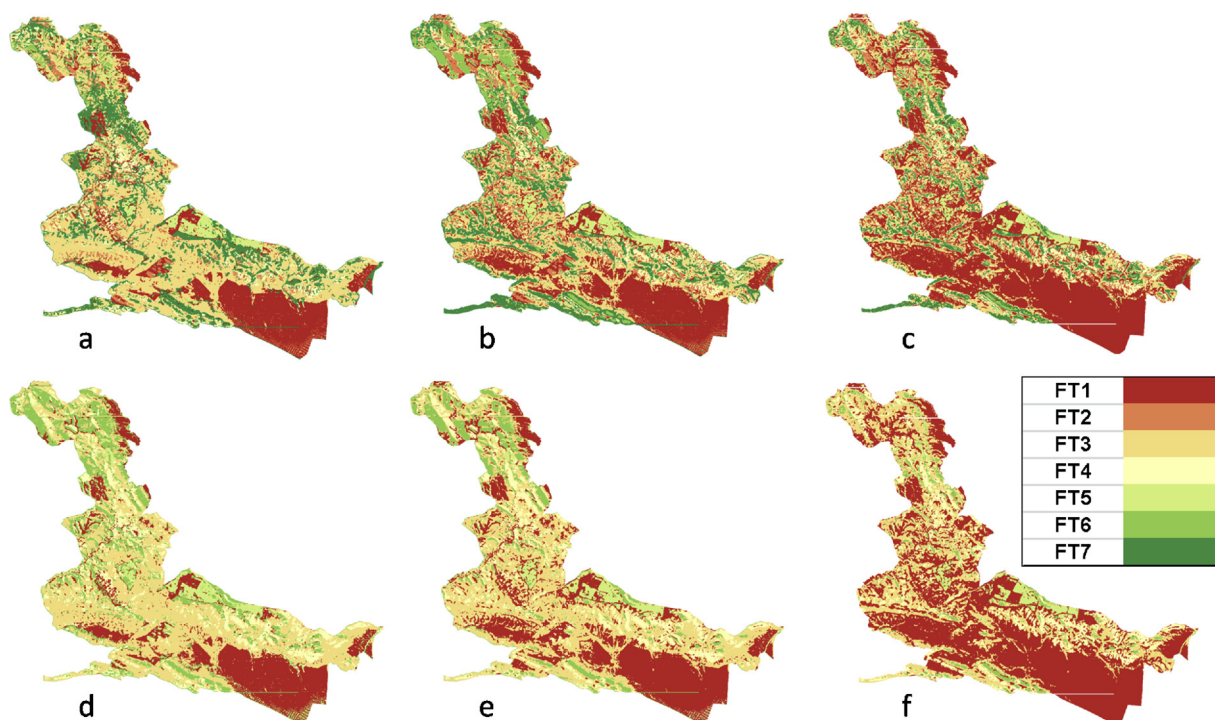
Fig. 5. Seven-FT (a, b, c) and five-FT (d, e, f) classifications using Approach 2 with SMA (a, d), SAM (b, e) and MESMA (c, f).

Table 5
Classification accuracy (%) considering the three spectral map methods, the two endmember selection approaches and the three datasets for validation.

		Approach 1		Approach 2	
		7FT	5FT	7FT	5FT
Riano's map	**SMA**	26	35	39	47
	SAM	24	38	36	45
	MESMA	27	41	32	37
CLM's map	**SMA**	NA	35	NA	55
	SAM	NA	41	NA	54
	MESMA	NA	45	NA	45
Fieldwork	**SMA**	25	40	36	44
	SAM	28	40	28	40
	MESMA	31	44	18	25

procedures to adjust adjacent pixels may improve the results (Ranganath and Shiva, 1985), but this issue is beyond the scope of this research. In addition, all of our validation maps have errors. Riaño's map is based on optical data that was only indirectly related to vegetation structure. CLM's map was based on the same LiDAR used for this analysis, together with optical data but their field work was collected in 2016. Therefore, this seven years gap between LiDAR and fieldwork in the validation data also affects the accuracy of their results. Despite all of these discrepancies, the confusion matrix for these two maps in comparison to the 2000 field data showed similar accuracies to those shown in Table 5, with accuracies of 42% and 38% for Riaño's and CLM's map respectively.

The LiDAR data has a very low point density of just 0.5 point/m^2, which probably misses shrubs and trees, underestimating their height (Evans et al., 2009). A higher density LiDAR point data provides more accurate VVP and is expected to considerably improve the precision of the results (García et al., 2011). Lastly, VVP is calculated by the proportion of bins by height strata which may be problematic because taller canopies reduce the number of returns from lower height strata. Other approaches may solve this issue, such as, calculating canopy cover by strata, defining profile curves like L moments, using skew and

kurtosis or using the FUSION profiling tool to improve correlations. Another factor with regard to the LiDAR data is that the pixel grid size (i.e. 30 m) was selected to make it coincident with one of the comparison dataset (i.e. Riaño's map). Due to this low point density of the LiDAR data, a bigger data grid would be more appropriate to ensure that enough points fall within each pixel. Even if the total number of returns within a pixel is sufficient within a 30 m grid, once this pixel is stratified into height intervals the total number of returns per stratum is low. Adoption of larger grid cells may result in higher fuels variability within each cell.

The methodology applied here is based solely on LiDAR data. Previous results have discriminated FTs using LiDAR data combined with optical remote sensing data (Marino et al., 2016; Jakubowski et al., 2013; Mutlu et al., 2008). The synergy of structural information from LiDAR together with spectral information from passive remote sensing data could improve the accuracy of the results. For instance, a grass FT (e.g. FT1) of the same height as a shrub FT (e.g. FT2) may have the same VVP signal however they are likely to be spectrally different. In contrast, two different shrub FTs may have the same spectral signature but different VVP profiles because their heights are different (Gajardo et al., 2014).

6. Conclusions

Originally developed to classify passive remote sensing data, the present study demonstrated the usefulness of several spectral mapping methods (i.e. SMA, SAM, and MESMA) applied to LiDAR data. The correlations were found using three different datasets for validation (i.e. Riaño's map, CLM's map and field data) corroborating the potential to retrieve FTs. A LiDAR signature library was developed to characterize FTs using the VVP from two different approaches. One based on field data and the second based on exploring spectral patterns in VVP. The Approach 2 for endmember selection rendered the highest overall accuracy, using maps of five-FTs and SMA as the spectral mapping method. This study is the first to apply spectral methods to characterize LiDAR data into FT classes. The results are promising, however given several sources of errors (e.g. time gaps between field

Table 6
Confusion matrices between the three spectral map methods for seven-FT classifications using the Approach 1 for the endmember selection and the 2000 fieldwork.

	SMA_FT1	SMA_FT2	SMA_FT3	SMA_FT4	SMA_FT5	SMA_FT6	SMA_FT7	Accuracy
F_FT1	5	2	3	1	0	0	1	41.67
F_FT2	2	3	4	1	0	0	0	30.00
F_FT3	2	7	14	2	2	0	2	48.28
F_FT4	0	4	20	4	1	0	5	11.76
F_FT5	0	3	5	1	0	0	6	0.00
F_FT6	0	5	3	0	0	0	9	0.00
F_FT7	1	3	0	0	0	0	5	55.56
Total								**24.6**

	SAM_FT1	SAM_FT2	SAM_FT3	SAM_FT4	SAM_FT5	SAM_FT6	SAM_FT7	Accuracy
F_FT1	9	0	2	1	0	0	0	75.00
F_FT2	3	3	2	2	0	0	0	30.00
F_FT3	2	9	11	4	2	0	1	37.93
F_FT4	0	11	3	8	2	5	5	23.53
F_FT5	3	5	1	1	0	0	5	0.00
F_FT6	1	4	2	2	1	0	7	0.00
F_FT7	1	4	0	0	0	0	4	44.44
Total								**27.78**

	MESMA_FT1	MESMA_FT2	MESMA_FT3	MESMA_FT4	MESMA_FT5	MESMA_FT6	MESMA_FT7	Accuracy
F_FT1	11	0	1	0	0	0	0	91.67
F_FT2	4	1	3	2	0	0	0	10.00
F_FT3	5	7	15	0	1	0	0	53.57
F_FT4	0	11	3	8	2	5	5	23.53
F_FT5	5	5	1	0	0	0	4	0.00
F_FT6	1	4	2	2	1	0	7	0.00
F_FT7	1	4	0	0	0	0	4	44.44
Total								**31.20**

Table 7
Confusion matrices between the three spectral map methods for seven-FT classifications using Approach 2 for the endmember selection and the 2000 fieldwork.

	SMA_FT1	SMA_FT2	SMA_FT3	SMA_FT4	SMA_FT5	SMA_FT6	SMA_FT7	Accuracy
F_FT1	10	1	1	0	0	0	0	83.33
F_FT2	3	2	5	0	0	0	0	20.00
F_FT3	5	0	22	0	0	0	2	75.86
F_FT4	2	3	17	5	0	1	6	14.71
F_FT5	3	1	2	0	1	1	7	6.67
F_FT6	0	1	3	0	3	0	10	0.00
F_FT7	1	1	2	0	0	0	5	55.56
Total								**35.71**

	SAM_FT1	SAM_FT2	SAM_FT3	SAM_FT4	SAM_FT5	SAM_FT6	SAM_FT7	Accuracy
F_FT1	9	0	2	1	0	0	0	75.00
F_FT2	3	3	2	2	0	0	0	30.00
F_FT3	2	9	11	4	2	0	1	37.93
F_FT4	0	11	3	8	2	5	5	23.53
F_FT5	3	5	1	1	0	0	5	0.00
F_FT6	1	4	2	2	1	0	7	0.00
F_FT7	1	4	0	0	0	0	4	44.44
Total								**27.78**

	MESMA_FT1	MESMA_FT2	MESMA_FT3	MESMA_FT4	MESMA_FT5	MESMA_FT6	MESMA_FT7	Accuracy
F_FT1	12	0	0	0	0	0	0	100.00
F_FT2	8	1	1	0	0	0	0	10.00
F_FT3	25	0	3	0	0	0	0	10.71
F_FT4	9	4	15	2	0	0	4	5.88
F_FT5	6	1	4	0	2	1	1	13.33
F_FT6	3	2	5	0	4	1	2	5.88
F_FT7	2	1	3	0	1	1	1	11.11
Total								**17.60**

data and LiDAR acquisition, the steep topography, and the low LiDAR point density) concurrent data sources should be considered for improving accuracies. Nonetheless, the accuracies obtained in this study for field work using SMA, MESMA, and SAM are higher than the official CLM map of fuel types.

Table 8

Confusion matrixes between the three spectral map methods for five-FTs classification using Approach 1 for the endmember selection and the 2000 field work.

	SMA_1	SMA_3	SMA_4	SMA_5	SMA_6	Accuracy
F_FT1	7	2	1	2	0	58.33
F_FT3	2	18	4	1	4	62.07
F_FT4	0	9	6	3	16	17.65
F_FT5	3	2	1	7	2	46.67
F_FT6	1	3	2	6	5	29.41
Total						**40.19**
	SAM_FT1	SAM_FT3	SAM_FT4	SAM_FT5	SAM_FT6	Accuracy
F_FT1	9	2	1	0	0	75.00
F_FT3	2	19	5	2	1	65.52
F_FT4	0	14	9	2	9	26.47
F_FT5	5	6	2	1	1	6.67
F_FT6	1	6	3	2	5	29.41
Total						**40.19**
	MESMA_FT1	MESMA_FT3	MESMA_FT4	MESMA_FT5	MESMA_FT6	Accuracy
F_FT1	11	1	0	0	0	91.67
F_FT3	5	21	1	1	0	75.00
F_FT4	0	14	9	2	9	26.47
F_FT5	6	6	1	1	1	6.67
F_FT6	1	6	3	2	5	29.41
Total						**44.34**

Table 9

Confusion matrixes between the three spectral map methods for five-FT classifications using Approach 2 for the endmember selection and the 2000 field work.

	SMA_1	SMA_3	SMA_4	SMA_5	SMA_6	Accuracy
F_FT1	10	1	0	1	0	83.33
F_FT3	6	19	0	0	4	65.52
F_FT4	1	20	9	0	4	26.47
F_FT5	2	1	2	2	8	13.33
F_FT6	0	3	1	6	7	41.18
Total						**43.93**
	SAM_FT1	SAM_FT3	SAM_FT4	SAM_FT5	SAM_FT6	Accuracy
F_FT1	9	2	1	0	0	75.00
F_FT3	2	19	5	2	1	65.52
F_FT4	0	14	9	2	9	26.47
F_FT5	5	6	2	1	1	6.67
F_FT6	1	6	3	2	5	29.41
Total						**40.19**
	MESMA_FT1	MESMA_FT3	MESMA_FT4	MESMA_FT5	MESMA_FT6	Accuracy
F_FT1	12	0	0	0	0	100.00
F_FT3	25	3	0	0	0	10.71
F_FT4	10	18	6	0	0	17.65
F_FT5	7	4	0	3	1	20.00
F_FT6	3	6	1	5	2	11.76
Total						**24.53**

the Cabañeros FTs map for comparison with this study.

References

Albini, F.A., 1976. Estimating Wildfire Behavior and Effects. USDA, Forest Service, Intermountain Forest and Range Experiment Station, Ogden.

Andersen, H., McGaughey, R.J., Reutebuch, S.E., 2005. Estimating forest canopy fuel parameters using LIDAR data. Remote Sens. Environ. 94, 4414–4449.

Burgan, R.E., Shasby, M.B., 1984. Mapping broad-area fire potential from digital fuel, terrain and weather data. J. For. 88, 228–231.

Congalton, R.G., Green, K., 1999. Assessing the Accuracy of Remotely Sensed Data: Principles and Practices. Lewis, Boca Raton, FL.

Dennison, P.E., Roberts, D.A., 2003. Endmember selection for multiple Endmember spectral mixture analysis using Endmember average RSME. Remote Sens. Environ. 87, 123–135.

Dennison, P.E., Halligan, K.Q., Roberts, D.A., 2004. A comparison of error metrics and constraints for multiple endmember spectral mixture analysis and spectral angle mapper. Remote Sens. Environ. 93, 359–367.

Erdody, T.L., Moskal, L.M., 2010. Fusion of lidar and imagery for estimating forest canopy fuels. Remote Sens. Environ. 114, 725–737.

Evans, J.S., Hudak, A.T., Faux, R., Smith, A.M.S., 2009. Discrete return lidar in natural resources: recommendations for project planning, data processing, and deliverables. Remote Sens. 1, 776–794.

Gajardo, J., García, M., Riaño, D., 2014. Applications of airborne laser scanning in Forest fuel assessment and fire prevention. In: In: Maltamo, M., Næsset, E., Vauhkonen, J. (Eds.), Forestry Applications of Airborne Laser Scanning: Concepts and Case Studies, Managing Forest Ecosystems 27. Dordrecht, Springer Science+ Business Media, pp. 439–462.

García, M., Riaño, D., Chuvieco, E., Salas, F.J., Danson, F.M., 2011. Multispectral and LiDAR data fusion for fuel type mapping using support vector machine and decision rules. Remote Sens. Environ. 115, 1369–1379.

Hermosilla, T., Ruiz, L.A., Kazakova, A., Coops, N., Moskal, L., 2014. Estimation of forest structure and canopy fuel parameters from small-footprint full-waveform LiDAR data. Int. J. Wildland Fire 22, 224–233.

Jakubowski, M.K., Guo, Q., Collins, B., Stephens, S., Kelly, M., 2013. Predicting surface fuel models and fuel metrics using lidar and CIR imagery in a dense, mountainous Forest. Photogramm. Eng. Remote Sens. 79, 37–49.

Jia, G.J., Burke, I.C., Goetz, A.F.H., Kaufmann, M.R., Kindel, B.C., 2006. Assessing spatial patterns of forest fuel using AVIRIS data. Remote Sens. Environ. 102, 318–327.

Kraus, K., Pfeifer, N., 1998. Determination of terrain models in wooded areas with airborne laser scanner data. ISPRS J. Photogramm. Remote Sens. 53, 193–203.

Kruse, F.A., Lefkoff, A.B., Boardman, J.W., Heidebrecht, K.B., Shapiro, A.T., Barloon, P.J., et al., 1993. The spectral image-processing system (sips)-interactive visualization and analysis of imaging spectrometer data. Remote Sens. Environ. 44, 145–163.

Lasaponara, R., Lanorte, A., Pignatti, S., 2006. Characterization and mapping of fuel types for the Mediterranean ecosystems of pollino national Park in Southern Italy by using hyperspectral MIVIS data. Earth Interact. 10, 1–10.

Marino, E., Ranz, P., Tomé, J.L., 2016. Generation of high-resolution fuel model maps from discrete airborne laser scanner and landsat-8 OLI: a low-cost and highly updated methodology for large areas. Remote Sens. Environ. 187, 267–280.

Mutlu, M., Popescu, S.C., Stripling, C., Spencer, T., 2008. Mapping surface fuel models using lidar and multispectral data fusion for fire behavior. Remote Sens. Environ. 112, 274–285.

Peterson, B., Nelson, K.J., Seielstad, C., Stoker, J., Jolly, W.M., Parsons, R., 2015. Automated integration of lidar into the LANDFIRE product suite. Remote Sensing Letters 6, 247–256.

PROMETHEUS, S.V. Project, 1999. Management Techniques for Optimisation of Suppression and Minimization of Wildfire Effects. System Validation. European Commission Contract number ENV4-CT98-0716.

Pyne, S.J., 1996. Introduction to wildland fire. Fire Management in the United States. John Wiley & Sons, New York.

Ranganath, H.S., Shiva, G., 1985. Correlation of adjacent pixels for multiple image registration. IEEE Tras. Comput. 7, 674–677.

Riaño, D., Chuvieco, E., Salas, J., Palacios-Orueta, A., Bastarrika, A., 2002. Generation of fuel type maps from landsat TM images and ancillary data in Mediterranean ecosystems. Can. J. For. Res.-Revue Canadienne De Recherche Forestiere 32, 1301–1315.

Riaño, D., Meier, E., Allgower, B., Chuvieco, E., Ustin, S.L., 2003. Modeling airborne laser scanning data for the spatial generation of critical forest parameters in fire behavior modeling. Remote Sens. Environ. 86, 177–186.

Riaño, D., Valladares, F., Condes, S., Chuvieco, E., 2004. Estimation of leaf area index and covered ground from airborne laser scanner (Lidar) in two contrasting forests. Agric. For. Meteorol. 124, 269–275.

Riaño, D., Chuvieco, E., Ustin, S.L., Salas, J., Rodríguez-Pérez, J.R., Ribeiro, L.M., et al., 2007. Estimation of shrub height for fuel-type mapping combining airborne LiDAR and simultaneous color infrared ortho imaging. Int. J. Wildland Fire 16, 341–348.

Roberts, D.A., Gardner, M., Church, R., Ustin, S., Scheer, G., Green, R.O., 1998. Mapping Chaparral in the Santa Monica mountains using multiple endmember spectral mixture models. Remote Sens. Environ. 65, 267–279.

Roberts, D.A., Dennison, P.E., Gardner, M.E., Hetzel, Y., Ustin, S.L., Lee, C.T., 2003. Evaluation of the potential of hyperion for fire danger assessment by comparison to the airborne vsible/infrared imaging spectrometer. Geosci. Remote Sens., IEEE Trans. 41, 1297–1310.

Roberts, D., Halligan, K., Dennison, P., 2007. ViperTools. http://www.vipertools.org/.

Rothermel, R.C., 1972. A Mathematical Model for Predicting Fire Spread in Wildland Fuels, Ogden, Utah. USDA Forest Service, Research Paper INT-115, Intermountain Forest and Range Experiment Station, Ogden, Utah, pp. 1–40.

Scott, J.H., Burgan, R.E., 2005. Standard Fire Behavior Fuel Models: A Comprehensive Set for Use with Rothermel's Surface Fire Spread Model, Fort Collins, Colorado. General Technical Report, Rocky Mountain Research Station, Fort Collins, Colorado, pp. 72.

Smith, M.O., Ustin, S.L., Adams, J.B., Gillespie, A.R., 1990a. Vegetation in deserts I. A regional measure of abundances from multispectral images. Remote Sens. Environ. 31, 1–26.

Smith, M.O., Ustin, S.L., Adams, J.B., Gillespie, A.R., 1990b. Vegetation in deserts II. Environmental influences on regional abundance. Remote Sens. Environ. 31, 27–52.

Valbuena, R., Mauro, F., Arjonilla, F.J., Manzanera, J.A., 2011. Comparing airborne laser scanning imagery fusion methods based on geometric accuracy in forested areas. Remote Sensing Environment 115, 1942–1954.

van Wagtendonk, J.W., Root, R.R., 2003. The use of multi-temporal landsat normalized difference vegetation index (NDVI) data for mapping fuel models in yosemite national Park, USA. Int. J. Remote Sens. 24, 1639–1651.

Zhao, K., Popescu, S., Meng, X., Pang, Y., Agca, M., 2011. Characterizing forest canopy structure with lidar composite metrics and machine learning. Remote Sens. Environ. 115, 1978–1996.